Chemical synthesis and ^{1}H-NMR 3D structure determination of AgTx2-MTX chimera, a new potential blocker for Kv1.2 channel, derived from MTX and AgTx2 scorpion toxins

CYRIL PIMENTEL,[1,4] SARRAH M'BAREK,[2,4] VIOLETTA VISAN,[3] STEPHAN GRISSMER,[3] FRANÇOIS SAMPIERI,[2] JEAN-MARC SABATIER,[2] HERVÉ DARBON,[1] AND ZIAD FAJLOUN[2,5]

[1]Architecture et fonction des Macromolécules Biologiques (AFMB), Centre National de la Recherche Scientifique UMR6098, Aix-Marseille Universités, Parc Scientifique et Technologique de Luminy Case 932, 13288 Marseille Cedex 09, France
[2]ERT62, IFR Jean Roche, Faculté de Médecine Nord, Cedex 15, France
[3]Universität Ulm, 89081 Ulm, Germany

Abstract

Agitoxin 2 (AgTx2) is a 38-residue scorpion toxin, cross-linked by three disulfide bridges, which acts on voltage-gated K$^+$ (Kv) channels. Maurotoxin (MTX) is a 34-residue scorpion toxin with an uncommon four-disulfide bridge reticulation, acting on both Ca^{2+}-activated and Kv channels. A 39-mer chimeric peptide, named AgTx2-MTX, was designed from the sequence of the two toxins and chemically synthesized. It encompasses residues 1–5 of AgTx2, followed by the complete sequence of MTX. As established by enzyme cleavage, the new AgTx2-MTX molecule displays half-cystine pairings of the type C1–C5, C2–C6, C3–C7, and C4–C8, which is different from that of MTX. The 3D structure of AgTx2-MTX solved by ^{1}H-NMR, revealed both α-helical and β-sheet structures, consistent with a common α/β scaffold of scorpion toxins. Pharmacological assays of AgTx2-MTX revealed that this new molecule is more potent than both original toxins in blocking rat Kv1.2 channel. Docking simulations, performed with the 3D structure of AgTx2-MTX, confirmed this result and demonstrated the participation of the N-terminal domain of AgTx2 in its increased affinity for Kv1.2 through additional molecular contacts. Altogether, the data indicated that replacement of the N-terminal domain of MTX by the one of AgTx2 in the AgTx2-MTX chimera results in a reorganization of the disulfide bridge arrangement and an increase of affinity to the Kv1.2 channel.

Keywords: maurotoxin; agitoxin 2; scorpion toxin; K$^+$ channels; synthetic peptide; NMR; solution structure; molecular docking

Agitoxin 2 (AgTx2) is a 38-residues toxin that has been isolated from the venom of *leiurus quinquestriatus hebraeus* scorpion (Garcia et al. 1994). This toxin was shown to reversibly block voltage-gated K$^+$ channels (*Shaker* B, Kv1.1, Kv1.2, and Kv1.3) (Hidalgo and MacKinnon 1995; Lipkind and Fozzard 1997; Gao and Garcia 2003). MTX is another small toxin isolated from the venom of the scorpion *Scorpio maurus palmatus* (Kharrat et al. 1997). It is a basic, C-terminal amidated, 34-mer peptide cross-linked by four disulfide bridges. The solid-phase technique has been used to obtain synthetic MTX (sMTX), and it was found that both the natural and synthetic MTX are equally lethal to mice by ICV inoculation (LD$_{50}$ of 80 ng/mouse). sMTX has been shown to be active in the nanomolar range on both voltage-gated Kv1.2 and IKCa channels (Fajloun et al. 2000a). AgTx2 is cross-linked according to C1–C4, C2–C5, and C3–C6, while MTX possesses C1–C5, C2–C6, C3–C4, and C7–C8 disulfide bridge organization (vs. C1–C5, C2–C6, C3–C7, and C4–C8 for other K$^+$ channel-selective four-disulfide-bridged scorpion toxins) (Bontems et al. 1991; Darbon et al. 1999). MTX is the sole toxin that exhibits an uncommon disulfide bridge organization among the four-disulfide-bridged scorpion toxins (e.g., Pi1, Pi4, Pi7, and HsTX1) (Olamendi-Portugal et al. 1996; Rogowski et al. 1996; Lebrun et al. 1997; Savarin et al. 1999; Fajloun et al. 2000b,c; M'Barek et al. 2003a), but yet it adopts the classical α/β scaffold (Blanc et al. 1997; M'Barek et al. 2003b). This motif, from which arises the wide functional diversity of scorpion toxins, is mainly composed of a short α-helix connected to a β-sheet by two disulfide bridges. However, some equally Cys-stabilized α/β-motifs composed of three antiparallel β-strands and one α-helix are found in insect and plant defensins (Spelbrink et al. 2004) that acts on the Ca^{2+} channel.

Here, we used MTX as a molecular template to design and chemically synthesize a scorpion toxin-derived chimera cross-linked by four disulfide bridges, AgTx2-MTX. This peptide encompasses residues 1–5 of AgTx2 at its N terminus, and the sequence of MTX at its C terminus. The N-terminal portion of AgTx2 was chosen to form the N-terminal extremity of AgTx2-MTX, because this domain is structured as being part of the three-stranded β-sheet that could be observed in the 3D structure of AgTx2 in solution (Krezel et al. 1995). In this contribution, we describe the synthesis by an optimized Fmoc/t-butyl strategy (Merrifield 1986), disulfide bridge organization, 3D structure in solution by ^{1}H-NMR means, and electrophysiological activity on both the Ca^{2+}-activated intermediate conductance and voltage-gated K$^+$ channels subtypes (IKCa and Kv1.2, respectively). Because AgTx2-MTX was found to be highly potent in blocking the Kv1.2 channel, we detailed the AgTx2-MTX to the mammalian Kv1.2 channel interaction by computed docking simulations using the HADDOCK program (High Ambiguity Driven DOCKing program) in order to better understand the structural features responsible for this difference in bioactivity.

Materials and Methods

Materials

N-α-Fluoren-9-ylmethyloxycarbonyl (Fmoc)-L-amino acids, Fmoc-amide resin, and reagents used for chemical synthesis of AgTx2-MTX were purchased from Perkin-Elmer. Solvents were analytical grade products from SDS (Peypin). Trypsin and chymotrypsin were purchased from Sigma.

Solid-phase synthesis of AgTx2-MTX

The AgTx2-MTX was synthesized by a solid-phase method (Merrifield1986) using an automated peptide synthesizer (Model 433A, Applied Biosystems, Inc.). The peptide chain was assembled by stepwise synthesis on 0.3 mmol of Fmoc-amide resin (1% cross-linked; 0.65 mmol of amino group/g) using 1 mmol of Fmoc-amino acid derivatives (Kharrat et al. 1996). The side-chain protecting groups of trifunctional residues were: *tert*-butyl for Ser, Thr, Tyr, and Asp; trityl (Trt) for Cys and Asn; pentamethylchroman for Arg; and *tert*-butyloxycarbonyl for Lys. *N*-α-amino groups were deprotected by treatments with 18% and 20% (v/v) piperidine/*N*-methylpyrrolidone (NMP) for 3 and 8 min, respectively. The peptide-resin was washed with NMP (5 × 1 min), and then Fmoc-amino acid derivatives were coupled (20 min) as their hydroxybenzotriazole active esters in NMP (3.3-fold excess). After the peptide-chain assembly was completed and the N-terminal Fmoc group removed, the peptide-resin (ca. 2.1 g) was treated, under stirring, for 3 h at room temperature, with a mixture of trifluoroacetic acid (TFA)/H$_2$O/thioanisole/ethanedithiol (88:5:5:2, v/v) in the presence of crystalline phenol (2.5 g), in a final volume of 30 mL/g of peptide resin. The peptide mixture was filtered to remove the resin, and the filtrate was precipitated and washed twice in cold diethylether. The crude peptide was then pelleted by centrifugation (3000*g*; 10 min) and the supernatant was discarded. The peptide was finally dissolved in H$_2$O, freeze-dried, and lyophilized. The crude peptide was then dissolved in 0.2 M Tris-HCl buffer (pH 8.4) to a final concentration of ~2 mM in peptide, then gently stirred under air to allow folding/oxidation (48 h, 25°C). The AgTx2-MTX was purified to homogeneity by semipreparative reversed-phase high-pressure liquid chromatography (HPLC) (Perkin-Elmer, C18 Aquapore ODS 20 μm, 250 × 10 mm), by means of a 60-min

linear gradient from 0% to 35% of buffer B (0.08% [v/v] TFA/ acetonitrile) in buffer A (0.1% [v/v] TFA/H2O), at a flow rate of 6 mL/min ($\lambda = 230$ nm). The identity and high degree of homogeneity of the chimera (as well as of synthetic toxins), were verified by: (1) analytical C18 reversed-phase HPLC (Chromolith RP18, 5 μm, 4.6 $\times$ 100 mm) using a 40-min linear gradient from 0% to 60% of buffer B (0.08% [v/v] TFA/ acetonitrile) in buffer A (0.1% [v/v] TFA/H$_2$O), at a flow rate of 1 mL/min; (2) amino acid composition after hydrolysis (6 N HCl/2% [w/v] phenol, 20 h, 118°C, N2 atmosphere); (3) Edman sequencing; and (4) molecular mass analysis by matrix-assisted laser desorption ionization-time-of-flight (MALDI-TOF) mass spectrometry.

Assignment of half-cystine pairings of peptides

The peptides (600 μg) were each added to a mixture of 10% (w/w) of trypsin and chymotrypsin in 0.2 M Tris-HCl buffer (pH 7.4) (14 h, 37°C). The resulting peptide fragments were then separated by analytical reversed-phase HPLC (Chromolith RP18, 5 μm, 4.6 $\times$ 100 mm) in a 60-min linear gradient from 0% to 60% of buffer B (0.08% [v/v] TFA/acetonitrile) in buffer A (0.1% [v/v] TFA/H$_2$O), at a flow rate of 1 mL/min (230 nm). The peptide fragments were also analyzed by mass spectrometry (RP-DE Voyager, Perseptive Biosystems).

Electrophysiology

Cell

Stable transfected mammalian cell lines expressing either Kv1.2 (Kv1.2) channel were used (Grissmer et al. 1994). The cell lines were maintained in Dulbecco's modified Eagle's medium containing 4 mM L-glutamine, 1 mM sodium pyruvate, (GIBCO), 10% (v/v) heat-inactivated fetal calf serum (PAA). The tsA cell line expressing human IKCa1 (hIKCa1) channel was a kind gift from Dr. Devor (University of Pittsburg, Pennsylvania).

Electrophysiological recordings

All of the experiments were carried out at room temperature (22°C–25°C) using the whole-cell recording mode of the patch-clamp technique (Hamill et al. 1981; Rauer and Grissmer 1996). Cells were bathed with mammalian Ringer's solution containing (in millimolars): 160 NaCl, 4.5 KCl, 2 CaCl$_2$, 1 MgCl$_2$, and 10 HEPES (pH 7.4) (with NaOH), with an osmolarity of 290–320 mOsm. When peptides were applied, 0.1% bovine serum albumin was added to the Ringer's solution. A simple syringe-driven perfusion system was used to exchange the bath solution in the recording chamber. Electrodes were pulled from glass capillaries (Science Products) in three stages, and fire-polished to resistances measured in the bath of

2.5–5 MΩ. The internal pipette solution used for measuring voltage-gated K$^+$ currents contained (in millimolars): 155 KF, 2 MgCl$_2$, 10 HEPES, and 10 EGTA (pH 7.2) (with KOH), with an osmolarity of 290–320 mOsm. For measuring K$^+$ currents through IKCa1 channels, an internal pipette solution containing (in millimolars): 135 Kaspartate, 8.7 CaCl$_2$, 2 MgCl$_2$, 10 EGTA, 10 HEPES (pH 7.2) (with KOH), with an osmolarity of 290–320 mOsm, (free [Ca^{2+}]i = 10^{-6} M), was used. Membrane currents were measured with an EPC-9 patch-clamp amplifier (HEKA Elektronik) interfaced to a Macintosh computer running acquisition and analysis software (Pulse and PulseFit). Capacitive and leak currents were subtracted using the P/10 procedure. Series-resistance compensation (>80%) was used if the current exceeded 2 nA. The holding potential in all experiments was −80 mV. Data analysis was performed in IgorPro, and Kd values were deduced by fitting a modified Hill equation (Itoxin/Icontrol = 1/[1 + ([toxin]/Kd)]), with a Hill coefficient of 1, to normalized data points obtained at more than four different peptide concentrations. The value of each peptide concentration was the mean of at least three measurements.

NMR spectroscopy

Sample preparation

A 1 mM sample of synthetic AgTx2-MTX in 0.5 mL of H$_2$O/D$_2$O (90/10 by vol.) at pH 3.0 was used for NMR spectra recordings. The amide proton exchange rate was determined after lyophilization of this sample and dissolution in 100% D$_2$O.

NMR experiments

All ^{1}H spectra were recorded on a BRUKER DRX500 spectrometer equipped with a HCN probe, and self-shielded triple axis gradients were used. Two-dimensional NOESY and TOCSY spectra were acquired at 290 K and 300 K in order to solve assignment ambiguities. The spectra collected at 290 K provided the optimal resolution of overlapping NMR signals of AgTx2-MTX; therefore, this temperature was used for further studies of the protein. Two-dimensional spectra were acquired using states-TPPI method (Marion et al. 1989) to achieve F1 quadrature detection (Marion and Wüthrich 1983). The spectral width in both dimensions was 6000 Hz. NOESY and TOCSY experiments were recorded with 2048 data points for t2 and 512 points for t1 increments, with 64 transients per experiment. A DQF-COSY experiment was recorded with 4096 data points in t2 and 1024 data points in t1. Water suppression was achieved using presaturation during the relaxation delay (1.3 s), and during the mixing time in the case of NOESY experiments, or using a

Watergate 3-9-19 pulse train (Piotto et al. 1992) using a gradient at the magic angle obtained by applying simultaneous x-, y-, and z-gradients prior to detection. NOESY spectra were acquired using a mixing time of 80 ms. TOCSY was performed with a spin-locking field strength of 8 kHz and spin-lock time of 80 ms. The amide proton exchange experiments were recorded immediately after dissolution of the peptides in D_2O. A series of NOESY spectra with a mixing time of 80 ms were recorded at 290 K, the first one for 1 h, followed by spectra of 12 h each. Amide protons still giving rise to nuclear Overhauser effect (NOE) correlations after 40 h of exchange were considered as slowly exchanging and therefore engaged in a hydrogen bond.

Data processing

Spectra were processed with the XWIN-NMR version 2.1. The matrices were transformed to a final size of 2.048 points in the acquisition dimension and to 1.024 points in the other, except for a coupling constant determination for which a 8.192×1.024 matrix was used in the COSY spectrum. The signal was multiplied by a shifted sine bell window in both dimensions prior to a Fourier transform, and then a fifth-order polynomial baseline correction was applied.

Spectral analysis

Identification of amino acid spin systems and sequential assignment were achieved using the two-step standard strategy described by Wüthrich (1986) and applied with graphical software, XEASY (Bartels et al. 1995). The comparative analysis of COSY and TOCSY spectra recorded in water gave the spin system signatures of the protein. The spin systems were then sequentially connected using the NOESY spectra.

Experimental restraints

The assignment and integration of nOe data using manual integration in the XEASY software allowed us to obtain a list of volumes that were automatically translated into upper limit distances by the calibration routine of the ARIA software (Linge et al. 2003). The Φ torsion angles constraints resulted from the $^3J_{HN-H\alpha}$ coupling constant measurements that measured on the COSY spectrum. Alternatively, they have been estimated by the INFIT program (Szyperski et al. 1992). For a given residue, separated NOESY cross-peaks with the backbone amide proton in the $\omega2$ dimension were used. Several cross-sections through these cross-peaks were selected that exhibited a good signal-to-noise ratio. They were added up, and only those data points of the peak region that were above the noise level were retained. The left and right ends of the peak region were then brought to zero intensity by a linear baseline correction. After extending the baseline-corrected peak region with zeros on both sides, which is equivalent to over sampling in the time domain, an inverse Fourier transformation was performed. The value of the $^3J_{HN-H\alpha}$ coupling constant was obtained from the first local minimum. The Φ angles were restrained to $-120 \pm 40°$ for a $^3J_{HN-H\alpha} \geq 8$ Hz and to $-65 \pm 25°$ for a $^3J_{HN-H\alpha} \leq 6$ Hz. No angle constraint was assigned to a $^3J_{HN-H\alpha} = 7$ Hz, a value considered as ambiguous. Determination of the amide proton exchange rates led us to identify protons involved in hydrogen bonding. The oxygen partners were then identified by visual inspection of the preliminary calculated structures.

Structure calculations

The distance restraints (from measured NOE volumes), dihedral angles (from $^3J_{HN-H\alpha}$ coupling constants), restraints from disulfides bridges, and from hydrogen bonds were used in structural calculations to determine toxin conformation. These restraints were introduced as input in ARIA implemented in CNS 1.1. (Brunger et al. 1998). In the first run, the calculation was initiated using the NOESY peak list, dihedral angles restraints, and the assignment of experimentally determined disulfide bridges. This first run allowed us to correct NOE assignment and gave rise to a preliminary fold that was used to detect hydrogen-bond carbonyl partners. In the second run, distance restraints, dihedral angles, hydrogen bonds, and disulfide bridges were used. We calculated 100 structures in the final iteration and 50 structures were kept for minimization in water. The 20 best structures were finally kept as defining the conformation of AgTx2-MTX chimera. Visual analysis of the final selected structures was carried out with PyMOL software (DeLano Scientific) and the geometric quality of the resulting structures was assessed with PROCHECK 3.4 and PROCHECK-NMR software (Laskowski et al. 1993). The 3D structure of AgTx2-MTX was deposited at the Protein Data Bank (code 2Z3S). The assigned chemical shifts of the chimera are deposited at the BioMagResBank (BMRB accession number 15299).

Docking simulations

Docking simulations were made with HADDOCK (High Ambiguity Driven DOCKing) (Dominguez 2003), which allows one to drive the docking process with previously obtained experimental data such as mutagenesis or NMR chemical-shift perturbation. This software is a compilation of python script based on Aria (Linge et al. 2003) using CNS (Brunger et al. 1998) to calculate structure with various types of constraints. The docking takes place in three steps: a randomization of orientations and rigid body

energy minimization, a semi-rigid simulated annealing in torsion angle space, and a final refinement in Cartesian space with explicit solvent. In the first stage, HADDOCK randomly orientates the two partners and performs a rigid body energy minimization with rotation and translation of each molecule. In the second stage, the best solutions resulting from the preceding energy minimization are then refined with three steps of simulated annealing refinements. The first step optimizes the orientation of the partners; the second optimizes the configuration of side chains at the interface; and the third permits some conformational rearrangements, where both backbone and side chains are allowed to move. In the third and last stage, the structures are exposed to the solvent during a steepest descent energy minimization performed in an 8 Å shell of TIP3P water molecules. The resulting structures are then clustered according to their pairwise backbone RMSD at the interface. These clusters are analyzed and ranked according to

their average interaction energies (sum of E_{elec}, E_{vdw}, E_{ACS}) and their average buried surface area.

Results

Rationale

To design a scorpion toxin-derived chimera, we focused on AgTx2 and MTX, two small scorpion toxins active on Kv channels and reticulated by three and four disulfide bridges, respectively. Their amino acid sequences and half-cystine pairings are shown in Figure 1A. MTX display a "non-conventional" arrangement of the type C1–C5, C2–C6, C3–C4, C7–C8 (Fajloun et al. 2000a). Therefore, they appeared to be good candidates for the production of a chimeric peptide, since they possess variant disulfide bridge organizations, while they fold according to the same regular α/β scaffold of scorpion toxins (Bontems et al. 1991; Darbon
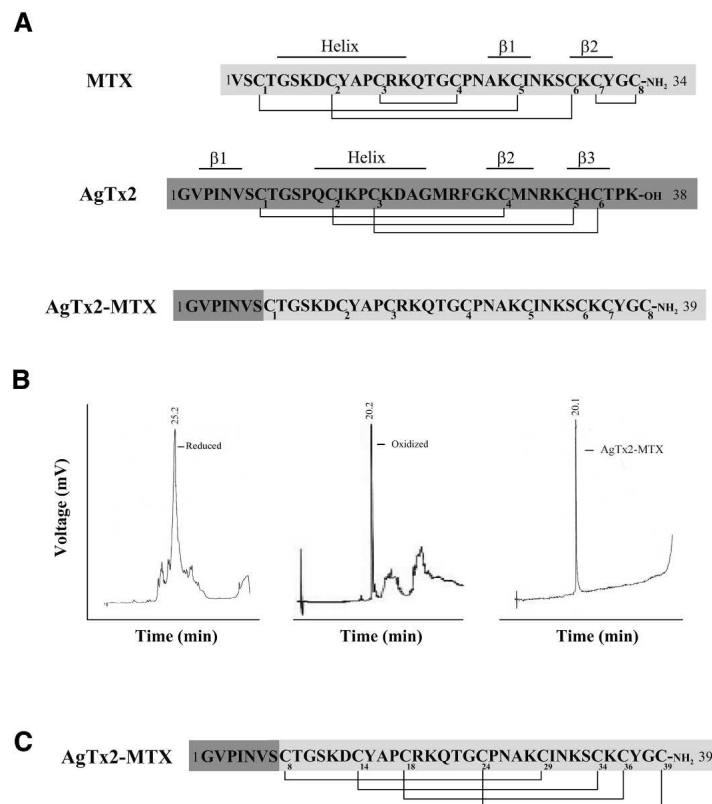
Figure 1. Sequence comparison between MTX, AgTx2, and AgTx2-MTX. Chemical synthesis and disulfide bridged organization of AgTx2-MTX chimera. (*A*) Amino acid sequences (one-letter code) and half-cystine pairings of MTX and AgTx2. Half-cystine residues are numbered by order of appearance from the N to the C terminus. The relative positioning of secondary structures (helix and β strands of the β-sheet structure) is indicated for each peptide. Disulfide bridges are depicted by solid lines. For AgTx2-MTX, the amino acid sequence of the 39-mer is shown. The amino acid sequence of this chimera derived from AgTx2 and MTX are shaded in dark and light gray, respectively. (*B*) AgTx2-MTX at different stages of its chemical synthesis. HPLC profiles of the crude reduced peptide (*left*), crude peptide after oxidative folding (*middle*), and purified AgTx2-MTX (*right*). (*C*) Half-cystine pairings of the AgTx2-MTX chimera. Assignment of the half-cystine pairings was achieved by analysis of the peptides yielded by enzyme cleavage (trypsin and chymotrypsin) of AgTx2-MTX.

et al. 1999). Moreover, AgTx2 and MTX display distinct profiles of pharmacological activities (high affinity of AgTx2 for Kv1.1, Kv1.3 channels, and high affinity of MTX for Kv1.2 channel). Since, contrary to MTX, AgTx2 possesses an extended N-terminal extremity (GVPINVS motif vs. VS motif of MTX), we added the N-terminal portion (residues 1–5) of AgTx2 to the N-terminal sequence of MTX to assess the global effect of the addition of this motif on MTX conformation and bioactivity. Figure 1A illustrates the amino acid sequences of MTX, AgTx2, and AgTx2-MTX chimeric peptide.

Synthesis and physicochemical characterization of AgTx2-MTX

Stepwise assembly of AgTx2-MTX was achieved on 0.30 mmol Fmoc-amide resin by means of optimized Fmoc/t-butyl chemistry (Merrifield 1986). Double-coupling of Fmoc-amino acids was used for the N-terminal portion of the chimera (residues 1–7). The overall yield of peptide chain assembly was 80%. The profiles of elution, by analytical C18 reversed-phase HPLC, of the crude reduced peptide after final acidolysis are shown in Figure 1B, left. The crude peptide was folded/oxidized by air exposure in Tris/HCl buffer (pH 8.3), for 72 h (Fig. 1B, middle), and the main oxidized product AgTx2-MTX was finally purified to >95% homogeneity by semipreparative HPLC (Fig. 1B, right). Mass spectrometry analysis of AgTx2-MTX gave an experimental Mr $(M+H)^+$ of 4420.2, in good agreement with the deduced Mr $(M+H)^+$ of 4420.5 for this chimera. Amino acid analysis of AgTx2-MTX after acidolysis provides an amino acid content that agreed with the calculated values. To determine the pattern of half-cystine connections, AgTx2-MTX was cleaved by a mixture of trypsin and chymotrypsin. The resulting proteolytic fragments were purified to homogeneity by HPLC and characterized by means of amino acid analysis, mass spectrometry, and Edman-sequencing techniques (data not shown). The half-cystine pairings were thereby mapped as Cys^8–Cys^{29}, Cys^{14}–Cys^{34}, Cys^{18}–Cys^{36}, and Cys^{24}–Cys^{39}. The four-disulfide-bridged organization of the MTX portion in AgTx2-MTX chimera corresponds to a "conventional" disulfide bridge organization of the type C1–C5, C2–C6, C3–C7, and C4–C8 (Pi1/Pi4/HsTx1 type) (Fig. 1C).

Pharmacology of AgTx2-MTX on IKCa and Kv1.2 channels

In patch-clamp experiments, we evaluated the effects of AgTx2, MTX, and AgTx2-MTX on human intermediate conductance Ca_{2+}-activated K_+ type 1 channel (hIKCa1) currents, expressed in tsA cell line (Fig. 2A). The three peptides fully inhibited hIKCa1 K_+ currents, with Kd values of 1152.48 ± 156 nM (AgTx2), 2.2 ± 0.13 nM (MTX), and
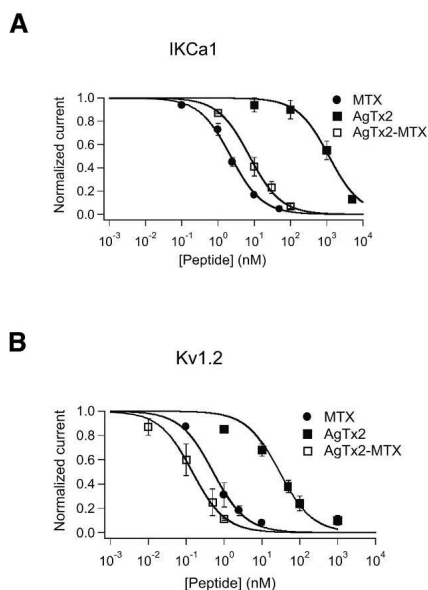
Figure 2. Pharmacological activity of AgTx2-MTX, AgTx2, and MTX. (*A*) Concentration-dependent inhibition curves of IKCa1 currents by AgTx2-MTX (□), AgTX2 (■), and MTX (●). Fits of the data yield IC_{50} values of 7.3 ± 0.6 nM (AgTx2-MTX), 2.2 ± 0.2 nM (MTX), and 1152 ± 156 nM (AgTx2) for IKCa1. (*B*) Concentration-dependent inhibition curves of Kv1.2 currents by AgTx2-MTX (□), AgTx2 (■), and MTX (●). Fits of the data yield IC_{50} values of 0.14 ± 0.01 nM (AgTx2-MTX), 0.51 ± 0.04 nM (MTX), and 26.8 ± 5.2 nM (AgTx2) for Kv1.2.

7.36 ± 0.62 nM (AgTx2-MTX). We observed that AgTx2 is thus 523-fold less active than MTX for interacting with hIKCa1, and AgTx2-MTX is thus 158-fold more active than AgTx2. This observation indicates that AgTx2 is not a specific ligand for IKCa1 and its N-terminal extremity does not affect the fixation of MTX on this channel. We also compared the effects of AgTx2, MTX, and AgTx2-MTX on K_+ currents from rat Kv1.2 channel (Fig. 2B). The Kd value obtained for AgTx2 is 26.8 ± 5.2 nM (Kv1.2). For MTX, it is 0.51 ± 0.04 nM (Kv1.2). The dose/response curves of current inhibition induced by AgTx2-MTX show a Kd value of 0.14 ± 0.01 nM for rat Kv1.2 channel. It thus appears that swapping the N-terminal VS motif of MTX by the GVPINVS motif of AgTx2 results in a 3.6-fold increase in blockage efficacy of Kv1.2 channel.

Structural properties of AgTx2-MTX

Determination of the 3D solution structure of AgTx2-MTX chimera

For NMR resonance assignment and secondary structures, the spin systems were identified on the basis of both COSY and TOCSY spectra. Once the sequential assignment was achieved, almost all protons were identified, and their resonance frequencies determined. The distribution of the $H\alpha_i/HN_{i+1}$, $H\beta_i/HN_{i+1}$, and HN_i/HN_{i+1}

NOE correlation and the coupling constants are presented in Figure 3A. Characteristic features of secondary structures such as α-helix and β-sheet have been found in AgTx2-MTX. The HN_i/HN_{i+1} correlations associated with hydrogen bonds and small coupling constants clearly demonstrate the presence of an α-helix, including residues Ser[11] to Gln[21], while strong $H\alpha_i/HN_{i+1}$ correlations, associated with large coupling constants indicate an extended region from Asn[26] to Tyr[37]. The structure of AgTx2-MTX was solved by using 516 NOE-based distance restraints, including 248 intra-residue, 158 sequential, 40 medium-range, and 70 long-range restraints. The distribution of these NOE is presented in Fig. 3B. In addition, included were 19 hydrogen bond restraints, derived from proton exchange, and 23 dihedral angle restraints, derived from the measurement of coupling constants, as well as 12 distance restraints derived from the disulfide bridges. Altogether, the final experimental set corresponded to 14.6 constraints per residue on average. The calculation using the whole set of restraints and water solvent minimization led to a single family of 20 structures. Structural statistics are given in Table 1. All of the solutions have good nonbonded contacts and good covalent geometry, as shown by the low values of CNS energy terms and low RMSD values for bond lengths,

valence, and improper dihedral angles. Correlation with the experimental data shows no NOE-derived distance violation greater than 0.2 Å. The analysis of the Ramachandran plot for the whole set of the 20 calculated structures reveals that 78.1% of the residues are in the most favored regions, 21.8% in the additional allowed regions, 0.2% in the generously allowed regions, and none in the disallowed regions (data not shown). The convergence of the 20 final structures (Fig. 4A) gives the three-dimensional structure of AgTx2-MTX, consisting of a compact disulfide-bonded core. This structure shows a typical α/β scaffold, in which an α-helix is connected to a three-stranded β-sheet by two disulfide bridges. In AgTx2-MTX chimera, the α-helix (Ser_{11} to Gln_{21}) is connected to the two strands of the β-sheet (Asn_{26} to Tyr_{37}) by the Cys[14]–Cys[34] and Cys[18]–Cys[36] disulfide bridges (Fig. 4B). These two strands are connected by a type II-β turn, like that described for MTX. Two others bridges stabilize the protein. One connects the N-terminal strand with the second one of the β-sheet (Cys[8]–Cys[29] bridge) and the other connects the C terminus with the loop located between the α-helix and the β-sheet (Cys[24]–Cys[34] bridge). The best-fit superimposition of the backbone traces of the 20 best structures is presented in Figure 4. The RMSD calculated on the whole structure is 1.43 Å for the backbone and 2.01 Å for all heavy atoms.
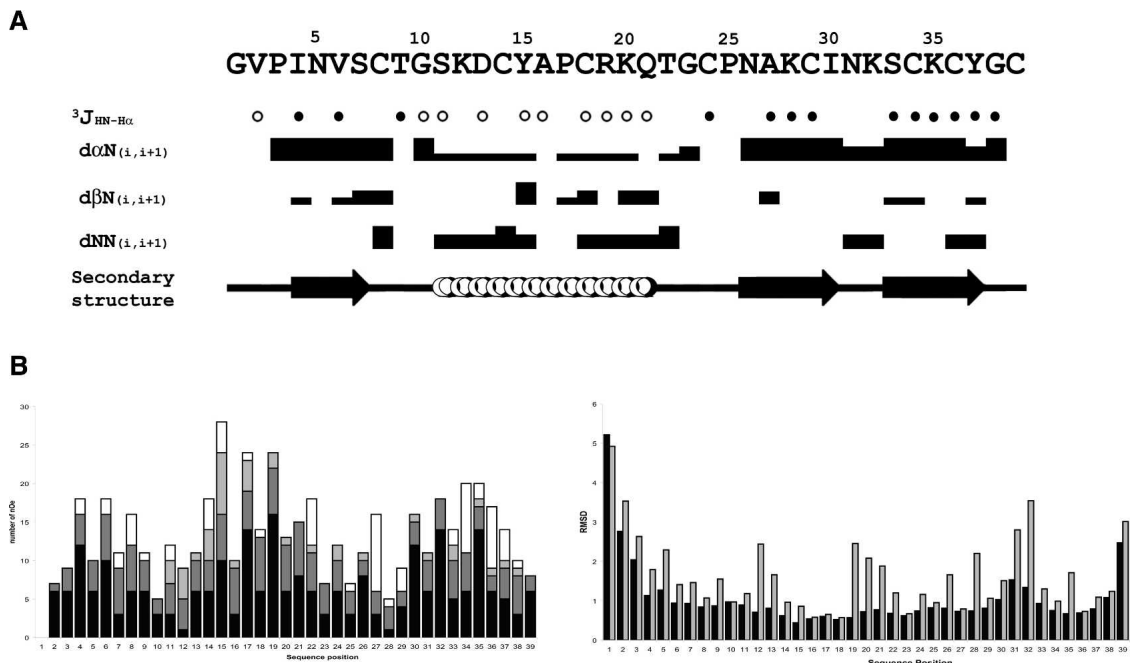
Figure 3. Statistical properties of AgTx2-MTX structure calculation. (*A*) Sequence of AgTx2-MTX and sequential assignments. Filled circles (●) represent $^3J_{HN-H\alpha}$ coupling constants ≥8 Hz and open circles (○) those ≤6 Hz. Collected sequential nOe are classified into strong, medium, and weak nOe, and are indicated by thick, medium, and thin lines, respectively. The last line indicates the secondary elements (extended regions). (*B*) nOe (*left*) and RMSD (*right*) distribution vs. sequence of AgTx2-MTX. Intraresidue nOe are in black, sequential nOe in dark gray, medium nOe in light gray, and long-range nOe in white. RMSD values for backbone and all heavy atoms are in black and gray, respectively.

Table 1. *Structural statistics of the 20 best structures of AgTx2-MTX*

RMSD (Å)	Residues 1–39	Residues 2–38
Backbone	1.43 ± 0.36	1.03 ± 0.21
All heavy atoms	2.01 ± 0.25	1.84 ± 0.23
Energies (kcal/mol)		
Total	−923.57 ± 46.90	
Bonds	9.82 ± 0.53	
Angles	46.55 ± 5.69	
Impropers	168.01 ± 28.24	
Dihedrals	176.27 ± 3.02	
van Der Waals (repel)	−72.069 ± 17.70	
Elec	−1252.15 ± 32.26	
nOe	13.737 ± 1.436	
Cdih	0.37 ± 0.19	
RMSD		
Bonds (Å)	0.0042 ± 0.0002	
Angles (°)	0.5473 ± 0.0322	
Impropers (°)	1.9947 ± 0.1685	
Dihedral (°)	40.64 ± 0.41	
nOe (Å)	0.0254 ± 0.0048	
Cdih (°)	0.8170 ± 0.2332	
RAMACHANDRAN		
Most favored and additional allowed (%)	99.8	
Generously allowed (%)	0.2	
Disallowed region (%)	0	

These values fall to 1.03 Å and 1.84 Å, respectively, if region 2–38 is solely considered. Despite the fact that the disulfide pattern is different for MTX and AgTx2-MTX, we observed that the fold is conserved for the common 34 amino acid residues. In a similar way, with a different sequence but an identical disulfide pattern, AgTx2-MTX adopts a fold very close to AgTx2. Together, these results suggest that a great number of residues of AgTx2-MTX have identical positions in MTX and/or AgTx2 (Fig. 5).

Docking of ChTX onto KcsA channel

In this study we first focused on the docking between charybdotoxin scorpion toxin (ChTX) with the KcsA potassium channel. Indeed, although docking methods are meant to propose structural models of bimolecular protein–protein or protein–ligand complexes, they do not guarantee that the resulting complexes will be close to the experimentally obtained solution by crystallography or NMR. Thus, in order to ensure that the used parameters are correctly set up, which is crucial for a correct interpretation of the obtained result, we first tested our docking methodology on an experimentally determined structure of protein–protein complex (Yu et al. 2005) (2A9H). It represents the only toxin–channel complex determined by direct structural information (NMR constraints). First, we made the docking calculation with the two proteins taken apart from the native complex and

randomly orientated. The experiment was made under constraint, which results in the positioning of lysine 27 in the center of the pore. This residue is conserved in all members of the α-KTX family. Therefore, the only experimental biological data in the docking computation was the position of the side chain of the critical lysine 27 as have been described in the literature (Park and Miller 1992b; Goldstein and Miller 1993; Fu et al. 2002) with mutagenesis or thermodynamic mutant cycle studies. The obtained solution was very close to the experimental complex, showing an RMSD at the interface <0.5 Å for α-carbons and 1.8 Å for all heavy atoms. With the aim of testing the capacity of the software to find the conformational changes taking place during the formation of the complex, another docking simulation was performed with the channel part issued from the complex (PDB code: 2A9H) and the 12 NMR solutions of ChTX taken from the Protein Data Bank (2CRD). This represented the real conditions in which we made the following docking simulations: Again, we found a solution close to the native complex. The RMSD of the interface for α-carbons is <1.3 Å and 2.3 Å for all heavy atoms. This approach provides convergent results close to the experimental complex, which allows us to use it to dock AgTx2-MTX chimera onto the potassium channel.

Docking of AgTx2, MTX, and AgTx2-MTX onto Kv1.2 channel

We performed the docking of the chimera onto the Kv1.2 channel because, with a Kd value of 0.14 nM, AgTx2-MTX
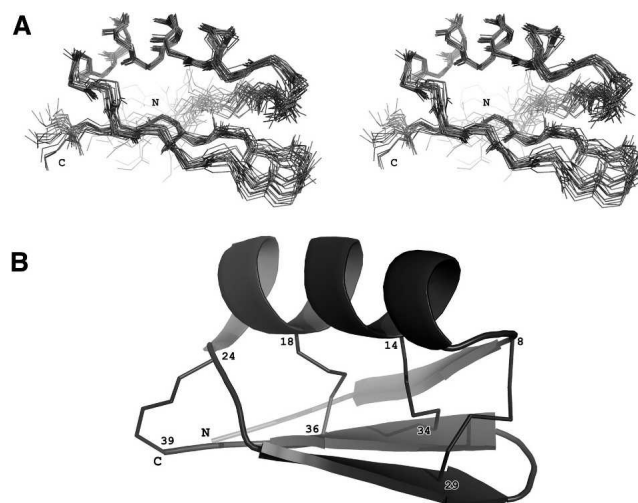
Figure 4. Structural properties of AgTx2-MTX. (*A*) Stereo pair view of the best fit of 20 structures of AgTx2-MTX. (*B*) PyMOL ribbon drawing of the averaged minimized AgTx2-MTX structure (DeLano Scientific). The eight half-cysteine residues are numbered according to their positions in the AgTx2-MTX amino acid sequence.
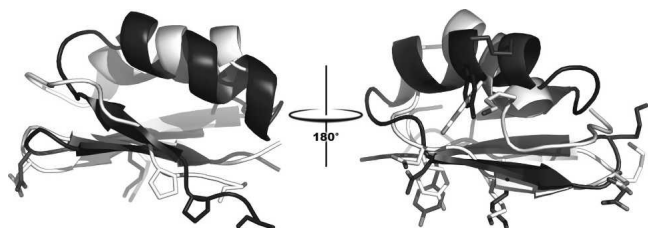
Figure 5. Structural alignment of AgTx2 with AgTx2-MTX (*left*) and MTX with AgTx2-MTX (*right*). Only amino acids conserved between the toxins and in interaction with the channel are shown.

was 3.6 times more active on Kv1.2 channels than MTX and 191 times more active than AgTx2. Furthermore, no other docking has already been made onto the recently elucidated structure of the mammalian potassium channel Kv1.2 (Long et al. 2005) (PDB ID: 2A79). For a better understanding of possible interactions responsible for such a high activity, we also performed the docking of AgTx2 and MTX onto the Kv1.2 channel beside that of AgTx2-MTX.

Docking simulations have often been driven according to constraints derived from biological data issued from the literature about critical residues involved in the toxin/channel interactions. The only constraint used in this work was the one derived from the conserved lysine responsible for the pore occlusion (Park and Miller 1992b; Goldstein and Miller 1993; Fu et al. 2002) (Lys[27] in AgTx2, Lys[23] in MTX, and Lys[28] in AgTx2-MTX). Docking simulations indicate that AgTx2, MTX, and AgTx2-MTX globally share a similar interaction map with Kv1.2 (Fig. 6), although some differences could be observed, which may explain their distinct blocking efficiency. All of these toxins seem to be stabilized onto the channel by sharing contacts with both the pore entryway residues and the external vestibule of the channel. First, the side chain of the central lysine residue of the β-sheet makes several hydrogen bonds with the carbonyl group of pore residues Gly[376] and Tyr[377]. Furthermore, the orientation of either of the three toxins is similar and consists of an alignment of their β-sheet with the interface between two dimers of the channel. As a consequence, this presents residues Asn[30] of AgTx2, Asn[21] of MTX, and Asn[26] of AgTx2-MTX in front of the highly conserved Asp[363] of the channel. Such a residue contact pattern has been identified earlier for various toxins of the α-KTX family in experiments of thermodynamic mutant cycles (Hidalgo and MacKinnon 1995; Ranganathan et al. 1996; Yu et al. 2005), NOE contacts and chemical-shift perturbations (Yu et al. 2005), transferred cross-saturation (Keuchi et al. 2003), chemical-shift perturbations in solid-state NMR (Lange et al. 2006), and mutagenesis studies (Park and Miller 1992a; Krezel at al. 1995; Lange et al. 2006). Such an orientation of toxin molecules also implies that Arg[24] of AgTx2,

Arg[27] of MTX, and Arg[32] of AgTx2-MTX make salt bridges with the channel opposite Asp[363]. Another common feature between these toxins is the presence of an aromatic residue on the β-sheet (His[34] of AgTx2, Tyr[32] of MTX, and Tyr[37] of AgTx2-MTX), which makes several hydrophobic contacts with Gly[378] and Asp[379] of the pore entry and Val[381] of the adjacent monomer. This aromatic residue and the central lysine responsible for the pore occlusion form the so-called functional dyad (Dauplais et al. 1997; M'Barek et al. 2003a; Pimentel et al. 2006). These three toxins also have a lysine residue on the second strand of the β-sheet (Lys[32] of AgTx2, Lys[30] of MTX, and Lys[35] of AgTx2-MTX), which makes salt bridges with the Asp[355] of the extracellular loop, even if this lysine does not have exactly the same position in the β-strand. It should be noted that Lys[32] and Lys[35] of AgTx2-MTX correspond to Lys[27] and Lys[30] of MTX, two residues that have been shown to play a pivotal role for MTX bioactivity, including its recognition of the Kv1.2 channel.

Several strong interactions are present in the complexes MTX/Kv1.2 and AgTx2-MTX/Kv1.2, while they are lacking in the AgTx2/Kv1.2 complex. This could explain the increase of 191-fold in affinity of these toxins. One of the major differences between MTX/AgTx2-MTX and AgTx2 is the presence of a lysine residue at the beginning of the α-helix (Lys[7] of MTX and Lys[12] of AgTx2-MTX), which makes a salt bridge with the Asp[355] of a channel extracellular loop. Another important difference is the
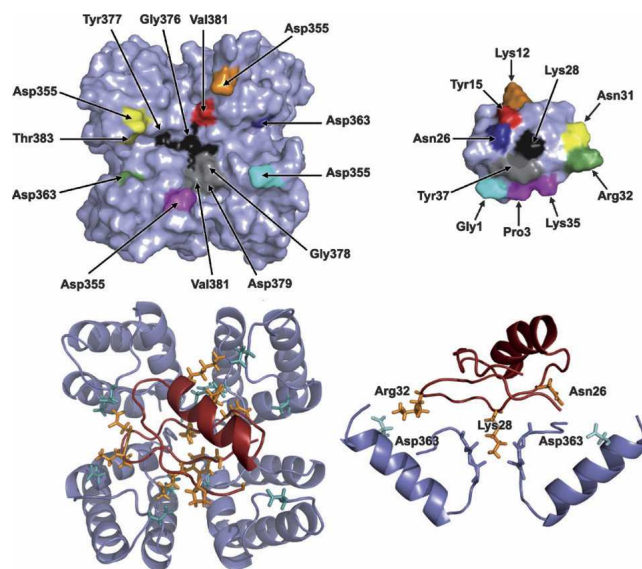
Figure 6. Important contacts (strong interaction) between AgTx2-MTX and Kv1.2 channel. Map detailing major molecular contacts between AgTx2-MTX and Kv1.2 channel (for clarity, not all the contacts are shown). The docking of AgTx2-MTX onto the Kv1.2 channel can be imagined by a 180° vertical rotation of AgTx2-MTX from *right* to *left*.

presence of a tyrosine residue on the α-helix (Tyr[10] of MTX and Tyr[15] of AgTx2-MTX), which makes hydrogen bonds with the close Val[381]. Finally, Asn[26] of MTX and Asn[31] of AgTx2-MTX make several hydrogen bonds with Asp[355] and Thr[383], while the corresponding residue Met[29] in AgTx2 makes only some hydrophobic contacts with Val[381] and Trp[366]. The chimera AgTx2-MTX presents some features derived from the AgTx2 toxin, such as the N-terminal part, which makes a third strand of the β-sheet. This five additional amino acids sequence permits us to enhance the affinity of the toxin in comparison to its counterpart MTX by allowing Gly[1] and Pro[3] of AgTx2-MTX to make several hydrogen bonds with Asp[355] residues of two adjacent monomers of the channel.

Discussion

The aim of this study was to evaluate whether it is possible to obtain novel reticulated peptides with variable pharmacological profiles with regard to the blockage of specific ion channel subtypes by using part of the amino acid sequences of scorpion toxins. Such an approach should help to unravel the molecular basis of the toxin recognition of ion channel through the production of various chimeric compounds, followed by careful investigation of their structural features and pharmacological properties. Our study was focused on AgTx2 and MTX scorpion toxins since, (1) AgTx2 has a conventional organization of the disulfide bridges associated at an extended N-terminal extremity, forming a third β−sheet, which does not exist in the MTX; (2) MTX has a short N-terminal extremity associated with atypical half-cystine pairing arrangement. Thus, we were curious to know which structural and pharmacological impact the grafting of the N-terminal extremity of AgTx2 onto MTX could have on the chimera AgTx2-MTX. By the herein described results, we showed that the replacement of the N-terminal VS motif of MTX by the N-terminal GVPINVS domain of AgTx2 within AgTx2-MTX resulted in a change of the MTX disulfide pairing pattern to the Pi1/Pi4/Pi7/HsTx1-like one. Such a change was previously observed to be induced by point mutations in the MTX structure (Fajloun et al. 2000b). Furthermore, we showed that the transfer of the N-terminal extremity affects the activity of the molecule on the Kv1.2 channel, on which the AgTx2-MTX chimera was found 191-fold more active than AgTx2 and 3.6-fold more active than MTX, which preserves its primary sequence within AgTx2-MTX. Such an increase in activity of blocking the Kv1.2 channel was previously observed with another chimera obtained by grafting the N-terminal extremity of Butantoxin (BuTX) to MTX (M'Barek et al. 2005). In the present work, we observed that AgTx2 was 523-fold less active than MTX for interacting with the human inter-

mediate conductance Ca^{2+}-activated channel (hIK-Ca1)—this was the first data evaluating AgTx2 activity regarding the hIKCa1—while AgTx2-MTX was 158-fold more active than AgTx2. These observations indicate that AgTx2 is not a specific ligand for IKCa1 and/or its N-terminal extremity does not affect the fixation of MTX on this channel.

From a structural properties point of view, the 3D structure of AgTx2-MTX solved in solution by ^{1}H-NMR showed that the conformation of AgTx2-MTX is similar to that of MTX (Blanc et al. 1997). As expected, the main structural difference between AgTx2-MTX and MTX relies on the existence of a third N-terminal β-strand, which, according to our docking simulations, carried out with 3D NMR structure of AgTx2-MTX and the 3D crystallography structure of Kv1.2, directly mediates the recognition of this channel. The 3D structure of AgTx2-MTX was used in docking simulations with the kv1.2 channel. The binding of the chimera seems to be stabilized over the channel pore by sharing contacts with residues of both the pore entryway and the extracellular loop. AgTx2-MTX appears to be stabilized onto the Kv1.2 channel by a number of close contacts (H-bonds and electrostatic interactions), in particular, Lys[12]/Asp[355], Tyr[15]/Val[381], Lys[28]/Gly[376], Asn[26]/Asp[363], Asn[31]/Asp[355], and Arg[32]/Asp[363] (Fig. 6). It should be noted that Lys[28] of AgTx2-MTX corresponds to Lys[23] of MTX, Lys27 of CTX, Lys22 of ShK, Lys25 of BgK, and Lys42 of KP4, a common basic residue that was shown to be pivotal for the scorpion toxin, sea anemone toxin, and plant defensin bioactivities (Goldstein et al. 1994; Rauer et al. 1999; Fajloun et al. 2000a,b; Gilquin et al. 2002; Spelbrink et al. 2004).

Moreover, the docking of AgTx2-MTX over Kv1.2 suggests that new specific residues peculiar to the structural AgTx2 domain of the chimera (e.g., Gly[1] and Pro[3]) contributed significantly to the chimera/channel interaction, thereby giving a structural basis of the strong blockade efficiency of this channel by the chimera. In light of these results, it seems that the high affinity of the chimera could result from a combination of, on one hand, new contacts established by the AgTx2 N-terminal domain (mainly a stabilization with extracellular loop) and, on the other hand, specific interactions that take place with the MTX moiety (mainly close contacts over the pore region).

Conclusion

We described herein the chemical synthesis of a four-disulfide-bridged peptide derived from the structures of two scorpion toxins (AgTx2 and MTX). The pharmacological properties (binding affinity and K^{+} current blockage efficacy) of the AgTx2-MTX chimera were evaluated

on both K^+ channel subtypes (IKCa and Kv1.2) and highlight some differences as compared with its natural counterparts. The implant of the N-terminal domain of AgTx2 onto MTX produced a chimera that was provided with a greater affinity for the Kv1.2 channel. Docking simulations that were achieved with the AgTx2-MTX NMR structure—determined in this work—and the crystallographic structure of Kv1.2, were performed and found to be in line with the experimental data. They suggest that new specific residues from the structural AgTx2 domain of the chimera (e.g., Gly[1] and Pro[3]) contributed significantly to the chimera/channel recognition, giving thereby a structural basis of the high-blockade efficiency of the chimera toward this channel. Therefore, we concluded that the replacement of the N-terminal VS motif of MTX by the GVPINVS domain of AgTx2 within AgTx2-MTX resulted in a change of the MTX-like disulfide pairing pattern to the Pi1/Pi4/Pi7/HsTx1like one. The structural outcome of this approach is also of interest, since the chimera still folds according to the canonical α/β scaffold. We conclude that a selective "gain of function" strategy represents an interesting way to produce toxin analogues or chimera with novel properties.

Acknowledgments

References

Bartels, C., Xia, T.H., Billeter, M., Guntert, P., and Wüthrich, K. 1995. The program XEASY for computer-supported NMR spectral analysis of biological macromolecules. *J. Biomol. NMR* **5:** 110–118.

Blanc, E., Sabatier, J.M., Kharrat, R., Meunier, S., El Ayeb, M., Van Reitschoten, J., and Darbon, H. 1997. Solution structure of maurotoxin, a scorpion toxin from *Scorpio maurus*, with high affinity for voltage-gated potassium channels. *Proteins* **29:** 321–333.

Bontems, F., Roumestand, C., Gilquin, B., Ménez, A., and Toma, F. 1991. Refined structure of charybdotoxin: Common motifs in scorpion toxins and insect defensins. *Science* **254:** 1521–1523.

Brunger, A.T., Adams, P.D., Clore, G.M., DeLano, W.L., Gros, P., Grosse-Kunstleve, R.W., Jiang, J.S., Kuszewski, J., Nilges, M., Pannu, N.S., et al. 1998. Crystallography & NMR system: A new software suite for macromolecular structure determination. *Acta Crystallogr. D Biol. Crystallogr.* **54:** 905–921.

Darbon, H., Blanc, E., and Sabatier, J.M. 1999. Animal toxins and potassium channels. In *Perspectives in drug discovery and design*. (eds. H. Darbon and J.M. Sabatier), Vol. 15, pp. 40–60. Kluwer/Dordrecht, The Netherlands.

Dauplais, M., Lecoq, A., Song, J., Cotton, J., Jamin, N., Gilquin, B., Roumestand, C., Vita, C., de Medeiros, C.L., Rowan, E.G., et al. 1997. On the convergent evolution of animal toxins. Conservation of a diad of functional residues in potassium channel-blocking toxins with unrelated structures. *J. Biol. Chem.* **272:** 4302–4309.

Dominguez, C. 2003. HADDOCK: A protein–protein docking approach based on biochemical and/or biophysical information. *J. Am. Chem. Soc.* **125:** 1731–1737.

Fajloun, Z., Ferrat, G., Carlier, E., Fathallah, M., Lecomte, C., Sandoz, G., di Luccio, E., Mabrouk, K., Legros, C., Darbon, H., et al. 2000a. Synthesis,

¹H-NMR structure, and activity of a three-disulfide-bridged maurotoxin analog designed to restore the consensus motif of scorpion toxins. *J. Biol. Chem.* **275:** 13605–13612.

Fajloun, Z., Carlier, E., Lecomte, C., Geib, S., di Luccio, E., Bichet, D., Mabrouk, K., Rochat, H., De Waard, M., and Sabatier, J.M. 2000b. Chemical synthesis and characterization of Pi1, a scorpion toxin from *Pandinus imperator* active on K^+ channels. *Eur. J. Biochem.* **267:** 5149–5155.

Fajloun, Z., Mosbah, A., Carlier, E., Mansuelle, P., Sandoz, G., Fathallah, M., di Luccio, E., Devaux, C., Rochat, H., De Waard, M., et al. 2000c. Maurotoxin *versus* Pi1/HsTx1 scorpion toxins. Toward new insights in the understanding of their distinct disulfide bridge patterns. *J. Biol. Chem.* **15:** 39394–39402.

Fu, W., Cui, M., Briggs, J.M., Huang, X., Xiong, B., Zhang, Y., Luo, X., Shen, J., Ji, R., Jiang, H., et al. 2002. Brownian dynamics simulations of the recognition of the scorpion toxin maurotoxin with the voltage-gated potassium ion channels. *Biophys. J.* **83:** 2370–2385.

Gao, Y.D. and Garcia, M.L. 2003. Interaction of agitoxin2, charybdotoxin, and iberiotoxin with potassium channels: Selectivity between voltage-gated and Maxi-K channels. *Proteins* **52:** 146–154.

Garcia, M.L., Garcia-Calvo, M., Hidalgo, P., Lee, A., and MacKinnon, R. 1994. Purification and characterization of three inhibitors of voltage-dependent K^+ channels from Leiurus quinquestriatus var. hebraeus venom. *Biochemistry* **33:** 6834–6839.

Gilquin, B., Racape, J., Wrisch, A., Visan, V., Lecoq, A., Grissmer, S., Menez, A., and Gasparini, S. 2002. Structure of the BgK-Kv1.1 complex based on distance restraints identified by double mutant cycles. Molecular basis for convergent evolution of Kv1 channel blockers. *J. Biol. Chem.* **277:** 37406–37413.

Goldstein, S.A. and Miller, C. 1993. Mechanism of charybdotoxin block of a voltage-gated K^+ channel. *Biophys. J.* **65:** 1613–1619.

Goldstein, S.A., Pheasant, D.J., and Miller, C. 1994. The charybdotoxin receptor of a *Shaker* K^+ channel: Peptide and channel residues mediating molecular recognition. *Neuron* **12:** 1377–1388.

Grissmer, S., Nguyen, A.N., Aiyar, J., Hanson, D.C., Mather, R.J., Gutman, G.A., Karmilowicz, M.J., Auperin, D.D., and Chandy, K.G. 1994. Pharmacological characterization of five cloned voltage-gated K^+ channels, types Kv1.1, 1.2, 1.3, 1.5, and 3.1, stably expressed in mammalian cell lines. *Mol. Pharmacol.* **45:** 1227–1234.

Hamill, O.P., Marty, A., Neher, E., Sakmann, B., and Sigworth, F.J. 1981. Improved patch-clamp techniques for high-resolution current recording from cells and cell-free membrane patches. *Pflugers Arch.* **391:** 85–100.

Hidalgo, P. and MacKinnon, R. 1995. Revealing the architecture of a K^+ channel pore through mutant cycles with a peptide inhibitor. *Science* **268:** 307–310.

Keuchi, K., Yokogawa, M., Matsuda, T., Sugai, M., Kawano, S., Kohno, T., Nakamura, H., Takahashi, H., and Shimada, I. 2003. Structural basis of the KcsA (K^+) channel and agitoxin2 pore-blocking toxin interaction by using the transferred cross-saturation method. *Structure* **11:** 1381–1392.

Kharrat, R., Mabrouk, K., Crest, M., Darbon, H., Oughideni, R., Martin-Eauclaire, M.F., Jacquet, G., El Ayeb, M., Van Rietschoten, J., Rochat, H., et al. 1996. Chemical synthesis and characterization of maurotoxin, a short scorpion toxin with four disulfide bridges that acts on K^+ channels. *Eur. J. Biochem.* **242:** 491–498.

Kharrat, R., Mansuelle, P., Sampieri, F., Crest, M., Oughideni, R., Van Rietschoten, J., Martin-Eauclaire, M.-F., Rochat, H., and El Ayeb, M. 1997. Maurotoxin, a four disulfide bridge toxin from *Scorpio maurus* venom: Purification, structure and action on potassium channels. *FEBS Lett.* **406:** 284–290.

Krezel, A.M., Kasibhatla, C., Hidalgo, P., MacKinnon, R., and Wagner, G. 1995. Solution structure of the potassium channel inhibitor agitoxin2: Caliper for probing channel geometry. *Protein Sci.* **4:** 1478–1489.

Lange, A., Giller, K., Hornig, S., Martin-Eauclaire, M.F., Pongs, O., Becker, S., and Baldus, M. 2006. Toxin-induced conformational changes in a potassium channel revealed by solid-state NMR. *Nature* **13:** 959–962.

Laskowski, R.A., MacArthur, M.W., Moss, D.M., and Thornton, J.M. 1993. A program to check the stereochemical quality of protein structures. *J. Appl. Crystallogr.* **26:** 283–291.

Lebrun, B., Romi-Lebrun, R., Martin-Eauclaire, M.-F., Yasuda, A., Ishiguro, M., Oyama, Y., Pongs, O., and Nakajima, T. 1997. A four-disulphide-bridged toxin, with high affinity towards voltage-gated K^+ channels, isolated from *Heterometrus spinnifer* (Scorpionidae) venom. *Biochem. J.* **328:** 321–327.

Linge, J.P., Habeck, M., Rieping, W., and Nilges, M. 2003. ARIA: Automated nOe assignment and NMR structure calculation. *Bioinformatics* **19:** 315–316.

Lipkind, G.M. and Fozzard, H.A. 1997. A model of scorpion toxin binding to voltage-gated K^+ channels. *J. Membr. Biol.* **158:** 187–196.

Long, S.B., Campbell, E.B., and Mackinnon, R. 2005. Crystal structure of a mammalian voltage-dependent Shaker family K$^+$ channel. *Science* **5:** 897–903.

Marion, D. and Wüthrich, K. 1983. Application of phase sensitive two-dimensional correlated spectroscopy (COSY) for measurements of ^{1}H-^{1}H spin-spin coupling constants in proteins. *Biochem. Biophys. Res. Commun.* **113:** 967–974.

Marion, D., Ikuto, M., Tschudin, R., and Bax, A. 1989. Rapid recording of 2D NMR spectra without phase cycling. Application to the study of hydrogen exchange in proteins. *J. Mag. Res.* **85:** 393–399.

M'Barek, S., Lopez-Gonzalez, I., Andreotti, N., Di Luccio, E., Visan, V., Grissmer, S., Judge, S., El Ayeb, M., Darbon, H., Rochat, H., et al. 2003a. A maurotoxin with constrained standard disulfide bridging: Innovative strategy of chemical synthesis, pharmacology, and docking on K$^+$ channels. *J. Biol. Chem.* **15:** 31095–31104.

M'Barek, S., Mosbah, A., Sandoz, G., Fajloun, Z., Olamendi-Portugal, T., Rochat, H., Sampieri, F., Guijarro, I., Mansuelle, P., Delepierre, M., et al. 2003b. Synthesis and characterization of Pi4, a scorpion toxin from *Pandinus imperator* that acts on K$^+$ channels. *Eur. J. Biochem.* **270:** 1–10.

M'Barek, S., Chagot, B., Andreotti, N., Visan, V., Mansuelle, P., Grissmer, S., Marrakchi, M., El Ayeb, M., Sampieri, F., Darbon, H., et al. 2005. Increasing the molecular contacts between maurotoxin and Kv1.2 channel augments ligand affinity. *Proteins* **15:** 401–411.

Merrifield, R.B. 1986. Solid phase synthesis. *Science* **232:** 341–347.

Olamendi-Portugal, T., Gomez-Lagunas, F., Gurrola, G.B., and Possani, L.D. 1996. A novel structural class of K$^+$-channel blocking toxin from the scorpion *Pandinus imperator. Biochem. J.* **315:** 977–981.

Park, C.S. and Miller, C. 1992a. Mapping function to structure in a channel-blocking peptide: Electrostatic mutants of charybdotoxin. *Biochemistry* **1:** 7749–7755.

Park, C.S. and Miller, C. 1992b. Interaction of charybdotoxin with permeant ions inside the pore of a K$^+$ channel. *Neuron* **9:** 307–313.

Pimentel, C., Choi, S.J., Chagot, B., Guette, C., Camadro, J.M., and Darbon, H. 2006. Solution structure PcFK1, a spider peptide active against *Plasmodium falciparum. Protein Sci.* **3:** 628–634.

Piotto, M., Saudek, V., and Sklenar, V. 1992. Gradient-tailored excitation for single-quantum NMR spectroscopy of aqueous solutions. *J. Biomol. NMR* **2:** 661–665.

Ranganathan, R., Lewis, J.H., and MacKinnon, R. 1996. Spatial localization of the K$^+$ channel selectivity filter by mutant cycle-based structure analysis. *Neuron* **16:** 131–139.

Rauer, H. and Grissmer, S. 1996. Evidence for an internal phenylalkylamine action on the voltage-gated potassium channel Kv1.3. *Mol. Pharmacol.* **50:** 1625–1634.

Rauer, H., Pennington, M., Cahalan, M., and Chandy, K.G. 1999. Structural conservation of the pores of calcium-activated and voltage-gated potassium channels determined by a sea anemone toxin. *J. Biol. Chem.* **274:** 21885–21892.

Rogowski, R.S., Collins, J.H., O'Neill, T.J., Gustafson, T.A., Werkman, T.R., Rogawski, M.A., Tenenholz, T.C., Weber, D.J., and Blaustein, M.P. 1996. Three new toxins from the *scorpion Pandinus imperator* selectively block certain voltage-gated K$^+$ channels. *Mol. Pharmacol.* **50:** 1167–1177.

Savarin, P., Romi-Lebrun, R., Zinn-Justin, S., Lebrun, B., Nakajima, T., Gilquin, B., and Menez, A. 1999. Structural and functional consequences of the presence of a fourth disulfide bridge in the scorpion short toxins: Solution structure of the potassium channel inhibitor HsTX1. *Protein Sci.* **8:** 2672–2685.

Spelbrink, R.G., Dilmac, N., Allen, A., Smith, T.J., Shah, D.M., and Hockerman, G.H. 2004. Differential antifungal and calcium channel-blocking activity among structurally related plant defensins. *Plant Physiol.* **135:** 2055–2067.

Szyperski, T., Guntert, P., Otting, G., and Wüthrich, K. 1992. Determination of scalar coupling constants by inverse Fourier transformation of in-phase multiples. *J. Magn. Reson. Imaging* **99:** 552–560.

Yu, L., Sun, C., Song, D., Shen, J., Xu, N., Gunasekera, A., Hajduk, P.J., and Olejniczak, E.T. 2005. Nuclear magnetic resonance structural studies of a potassium channel-charybdotoxin complex. *Biochemistry* **44:** 15834–15841.

Wüthrich, K. 1986. *NMR of proteins and nucleic acids*, pp. 2–199. John Wiley & Sons, New York.